AIAA JOURNAL
Vol. 32, No. 6, June 1994

Boundary Conditions for Unsteady Supersonic Inlet Analyses

David W. Mayer* and Gerald C. Paynter†
Boeing Commercial Airplane Group, Seattle, Washington 98124

New bleed and compressor face boundary conditions have been developed to improve the accuracy of unsteady supersonic inlet calculations. The new bleed boundary condition relates changes in the bleed hole discharge coefficient to changes in the local flow conditions; the local bleed flow rate can more than double as a shock moves forward over a bleed band in response to inlet flow disturbances. The stability margin of the inlet is strongly dependent on the throat bleed configuration since the locally rapid increase in bleed flow has a strong effect on the motion of the normal shock. The new compressor face boundary condition accounts for changes in the unsteady flow conditions at the compressor face by specifying the compressor face corrected mass flow or Mach number either as a constant or as a linear function of the stagnation conditions. The effects of inlet flow disturbances on the flow at the compressor face are represented more realistically with this new boundary condition than with traditional fixed static pressure or mass flow conditions. Euler calculations of the dynamic response of an inlet flow to a flow disturbance at the compressor face with 20- and 90-deg throat bleed hole angles are reported. These results indicate that an extra margin of stability for the inlet is obtained with 90-deg bleed holes because the increase in bleed flow rate as the shock moves forward over a bleed band is much larger for 90-deg holes than for 20-deg holes.

Nomenclature

A	= cross-sectional area
a	= speed of sound
D	= bleed hole diameter
E	= stagnation energy per unit volume
J	= Jacobian of the coordinate transformation
K_P	= empirical pressure coefficient, Eq. (7)
K_T	= empirical temperature coefficient, Eq. (7)
L	= bleed hole length
M	= Mach number
$\dot{m}$	= mass flux
$\boldsymbol{n}$	= flow domain outward unit normal vector
O	= order
P	= pressure
Q_{sonic}	= sonic mass flow coefficient, Eq. (3)
$\hat{Q}$	= vector of dependent variables
r	= radius
T	= temperature
t	= time
$\boldsymbol{t}$	= unit tangent vector, $u_1\hat{i}_1 + u_2\hat{i}_2$
$\boldsymbol{u}$	= velocity vector
x, y	= Cartesian coordinates
α	= angle of bleed holes relative to surface
δ	= P_T/P_{T_r}
ξ, η	= computational coordinates
γ	= ratio of specific heats
Φ	= surface porosity, Eq. (2)
ϕ	= arbitrary variable
ρ	= density
θ	= T_T/T_{T_r}

Subscripts

1, 2	= component in x or y direction
bleed	= at the bleed system
CF	= at the compressor face
c	= corrected value
i, j	= computational indices
lip	= at the cowl lip
local	= at the wall for inviscid flows or at the boundary-layer edge for viscous flows
max	= maximum value
min	= minimum value
plenum	= at the bleed plenum
r	= reference value
$S2$	= downstream side of throat shock
surface	= at the surface
T	= stagnation condition
t	= partial derivative with respect to time
wall	= at the wall
x, y	= partial derivatives with respect to x or y

Superscripts

n	= time plane
$'$	= dimensional quantity

Introduction

THE propulsion systems for new supersonic aircraft, such as the high-speed civil transport, require high performance supersonic inlets. These inlets must provide sufficient airflow to meet the demands of the propulsion system at a high-pressure recovery, low-flow distortion, and minimum drag penalty to the aircraft. Flow stability must be maintained to reduce the risk of an inlet unstart (i.e., to avoid expelling the normal shock from the inlet).

Since the compressor requires subsonic airflow, the inlet must decelerate the air to subsonic conditions. The initial deceleration is accomplished through a series of oblique shocks that terminate in a normal shock. To minimize total pressure losses across the normal shock, the inlet is designed to keep this shock just downstream of the inlet throat where the local Mach number is just slightly greater than one.

A primary inlet design goal is to maintain the normal shock in a stable position just downstream of the throat. If disturbances to the inlet flow (which may arise from an engine transient, from a transient in the freestream flow, or from moving geometry within the inlet) cause the normal shock to move upstream of the throat, the inlet will unstart. An inlet with a large stability margin will tolerate larger disturbances to the inlet flow without resulting in an unstart. The penalty for the large stability margin is typically a loss in total

Received April 9, 1993; revision received Sept. 13, 1993; accepted for publication Sept. 20, 1993.

*Senior Specialist Engineer, Propulsion Research Staff. Senior Member AIAA.

†Associate Technical Fellow, Propulsion Research Staff. Associate Fellow AIAA.

pressure recovery, increased distortion, and increased bleed drag. The penalty for an inlet unstart is a rapid and dramatic increase in drag, large control forces to maintain aircraft control, and the potential loss of aircraft control.

The shock/boundary-layer interactions can lead to boundary-layer separation, which reduces the pressure recovery, increases the flow distortion, and can also induce an inlet unstart. To prevent separation, the low-energy part of the boundary layer, near the wall, is often bled away through perforated or porous walls. The boundary-layer bleed in the throat also has a stabilizing influence on the normal shock: since the bleed rate can increase significantly behind the shock (due to the pressure rise across the shock and the change in bleed hole discharge coefficient), the forward motion of the normal shock is minimized.

Traditionally, much of the inlet performance information needed to design the inlet has been obtained from wind-tunnel tests. The rising costs of wind-tunnel testing have lead to an increased emphasis on computational fluid dynamic (CFD) analysis techniques. Improvements in computer speed and memory size now make it feasible to obtain inlet performance information (including the stability margin) using CFD techniques.

Although unsteady CFD codes exist, they typically do not include the necessary boundary conditions for analyzing unsteady inlet flows. The objective of this study was to devise improved bleed and compressor face boundary conditions for analyzing unsteady supersonic inlet flows with an existing Euler/Navier-Stokes code. Other researchers have developed bleed boundary conditions,[1,2] but these do not accurately account for the change in bleed mass flux as a shock moves over the bleed region. An improved bleed boundary condition was developed during the course of this study. In addition, a compressor face boundary condition was developed to account for unsteady flow conditions at the compressor face.

In the next section, a mixed-compression axisymmetric inlet configuration is described. Then a brief description of the flow solver used to analyze the inlet flow is provided, followed by descriptions of the new bleed and compressor face boundary conditions. Next, the new bleed and compressor face boundary conditions are demonstrated by calculating the response of the inlet flow following a 1% decrease in compressor face mass flow. The stability margins with 20- and 90-deg bleed holes in the throat region are compared. Conclusions based on this work with recommendations for future work are presented at the end of the article.

Supersonic Inlet Configuration

A mixed-compression translating centerbody inlet was used for the boundary condition development and is shown in Fig. 1. Detailed design information is contained in Ref. 3. The configuration had a length (measured from the centerbody tip to the compressor face) of 6.3 cowl-lip radii. The flow conditions are for a freestream Mach number of 2.35 at an altitude of 60,000 ft. Table 1 describes the bleed system. A bleed region consisted of two to four rows of staggered holes with a hole diameter approximately equal to the local boundary-layer displacement thickness just upstream of the bleed band. The holes were spaced between 2.0 and 2.2 hole diameters in a circumferential direction. Bleed plenum pressures were set to the freestream static pressure to insure that all of the bleed regions were choked. The bleed plenum pressure was assumed to be constant for this study so that the flow through a bleed region downstream of the inlet throat remained choked as the normal shock moved forward over the bleed region. The cowl slot was simulated by a porous wall section using discharge coefficient data for 20-deg bleed holes.

Flow Solver

The inlet flowfield calculations were performed with the PARC computer code distributed by the U.S. Air Force.[4] Detailed descriptions of the code are provided in Ref. 4, and only a brief summary of the significant features of the code is presented here. The PARC code is a general purpose flow analysis program based on the ARC code developed at NASA Ames. The code shares many of the features of the original ARC code and has been extensively

Table 1 Bleed system description

Bleed region	Area, A_{bleed}/A_{lip}	Angle, deg	Rows	Row or slot location, x/r_{lip}
Cowl 1	0.00473	20	2	3.1950–3.2349
Cowl 2	0.00462	20	2	3.3951–3.4367
Cowl 3	0.00449	20	2	3.5951–3.6349
Cowl slot	0.0030	——	——	3.7900–3.8300
Cowl 4	0.00760	20	4	3.8816–3.9425
Centerbody 1	0.0070	20	4	3.4167–3.4775
Centerbody 2	0.0055	20	4	3.6190–3.6670
Centerbody 3	0.0070	20	4	3.8175–3.8775

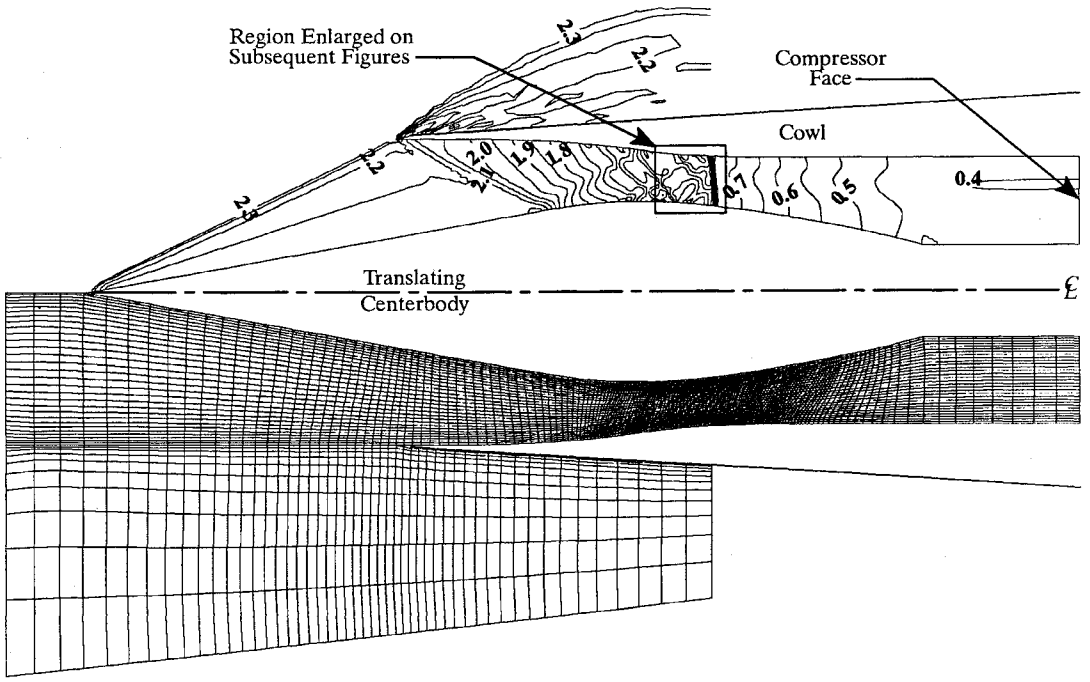

Fig. 1 Axisymmetric mixed-compression inlet. Upper half shows Mach contours; lower half shows computational grid.

enhanced for internal flows and for use in an applications-oriented environment.

The basis of the algorithm is the Reynolds-averaged Navier-Stokes equations for a Newtonian fluid that obeys the Fourier heat conduction law. These equations form a system of partial differential equations (i.e., continuity, momentum, and energy equations). The equations are cast in nondimensional conservation law form and then transformed into a general curvilinear coordinate system. The resulting vector of dependent variables is represented by

$$\hat{Q} = \frac{1}{J}\begin{bmatrix} \rho \\ \rho u_1 \\ \rho u_2 \\ E \end{bmatrix}$$

where the nondimensional variables are defined by

$$\rho \equiv \rho' / \rho'_r$$
$$u \equiv u' / a'_r$$
$$E \equiv E' / (\rho'_r \ a'^2_r)$$

and nondimensional distances, pressures, and temperatures are defined by

$$x \equiv x' / x'_r$$
$$P \equiv P' / (\rho'_r \ a'^2_r) \equiv P' / (\gamma P'_r)$$
$$T \equiv T' / T'_r$$

Central differences are used to cast the resulting system of equations into finite difference form. The equations are solved using the approximate factorization scheme developed by Beam and Warming, including the diagonalized implicit matrices developed by Pulliam. An alternate flow solver based on the multistage Runge-Kutta method is provided for accurate calculations of time-dependent flows. Implicit residual smoothing may be used to increase the time step size at the expense of reduced temporal accuracy.

Using PARC, complex geometries can be analyzed with relative ease due to the multiblock grid capability and the ability to easily specify boundary conditions on the interior as well as the boundaries of the grid blocks. Inviscid, laminar, and turbulent flows can be simulated for two-dimensional, axisymmetric, or three-dimensional geometries.

Bleed Boundary Condition

In supersonic inlets, mass is bled from the internal surfaces to prevent boundary-layer separation and to stabilize the throat normal shock. Accurate modeling of the dynamics of the inlet flow requires accurate modeling of the effect of bleed on the motion of the shock. Previous bleed boundary conditions assumed that the bleed flow rate was either fixed and independent of the shock position or that the flow rate varied but didn't account for changes in the bleed hole discharge coefficient. Since the discharge coefficient of the bleed holes changes depending on whether the local flow is supersonic or subsonic (i.e., upstream or downstream of the throat normal shock) and depending on vena contracta effects, the bleed boundary condition affects the motion of the normal shock in the throat, as noted by Paynter et al.[5]

The bleed boundary condition developed for this study treats each bleed region like a porous wall extending from the front edge of the bleed band to the aft edge. The flow velocity normal to the wall is computed based on the local flow properties, the total bleed hole area, and a discharge coefficient function. The boundary condition is applicable to both steady-state and time-accurate calculations, as well as for inviscid and viscous calculations (i.e., Euler and Navier-Stokes calculations).

The bleed boundary condition is a "global" model of the effects of bleed on the inlet. The model yields the overall effects of bleed mass removal on the inlet flow but does not completely model local variations in bleed that undoubtedly exist in either the streamwise or cross-stream direction. The model is based on the assumption that removing the correct amount of mass from the inlet as the normal shock moves forward over the simulated porous bleed region is much more important in an accurate simulation of the motion of the normal shock than how the mass flux removal is distributed over a bleed region.

The solution procedure for the bleed boundary condition starts with extrapolation of all of the PARC dependent variables (i.e., ρ, ρu_1, ρu_2, E) from values at time $n-1$ and n to time $n+1$. The procedure used to extrapolate the flow variables in space and time is based on a Taylor's series expansion for a function of three variables (i.e., t, x, and y) as follows:

$$\phi(t,x,y) = \phi(a,b,c) + (t-a)\,\phi_t(a,b,c) + (x-b)\,\phi_x(a,b,c) + (y-c)\,\phi_y(a,b,c) + O(\Delta t^2, \Delta x^2, \Delta y^2) \quad (1)$$

where the partial derivatives have been denoted using subscript notation, e.g., $\phi_t = \partial\phi/\partial t$. This equation is transformed from physical space to computational space (i.e., from x, y coordinates to ξ, η coordinates) using the following relationships:

$$\frac{\partial}{\partial x} = \xi_x \frac{\partial}{\partial \xi} + \eta_x \frac{\partial}{\partial \eta}$$

and

$$\frac{\partial}{\partial y} = \xi_y \frac{\partial}{\partial \xi} + \eta_y \frac{\partial}{\partial \eta}$$

where the transformation derivatives ξ_x, ξ_y, η_x, and η_y are the grid metrics. The partial derivatives are approximated using backward differences in time of $\mathcal{O}(\Delta t)$ and differences in space of $\mathcal{O}(\Delta x^2)$ and $\mathcal{O}(\Delta y^2)$. For example, the following equation is the finite difference expression used on a boundary on the right side of the computational domain (i.e., at $i = i_{\max}$):

$$\phi^{n+1}_{i,j} = \phi^n_{i-1,j} + (t^{n+1} - t^n)\left(\frac{\phi^n_{i-1,j} - \phi^{n-1}_{i-1,j}}{t^n - t^{n-1}}\right) + (x_{i,j} - x_{i-1,j})\left(\xi_x \frac{\phi^n_{i,j} - \phi^n_{i-2,j}}{2} + \eta_x \frac{\phi^n_{i-1,j+1} - \phi^n_{i-1,j-1}}{2}\right) + (y_{i,j} - y_{i-1,j})\left(\xi_y \frac{\phi^n_{i,j} - \phi^n_{i-2,j}}{2} + \eta_y \frac{\phi^n_{i-1,j+1} - \phi^n_{i-1,j-1}}{2}\right)$$

Note that this equation is a Taylor series expansion at $\phi^n_{i-1,j}$ and is used to obtain $\phi^{n+1}_{i,j}$. Similar expressions are used on the left, top, and bottom boundaries of the computational domain (i.e., at $i = i_{\min}$, $j = j_{\max}$, and $j = j_{\min}$, respectively).

For simplicity the time step size is assumed to be constant. Since variable time step sizes will introduce an error in the extrapolation procedure, constant time steps are used for time-accurate calculations. For steady-state calculations, the error due to variable time step size will effectively be zero once the steady-state solution is achieved.

Next the surface porosity is determined for the bleed boundary condition patch. The surface porosity is defined by the following formula:

$$\Phi = \frac{A_{\text{bleed}}}{A_{\text{surface}}} \quad (2)$$

where A_{bleed} is the total cross-sectional area of the bleed holes within the boundary condition patch, and A_{surface} is the surface area of the boundary condition patch.

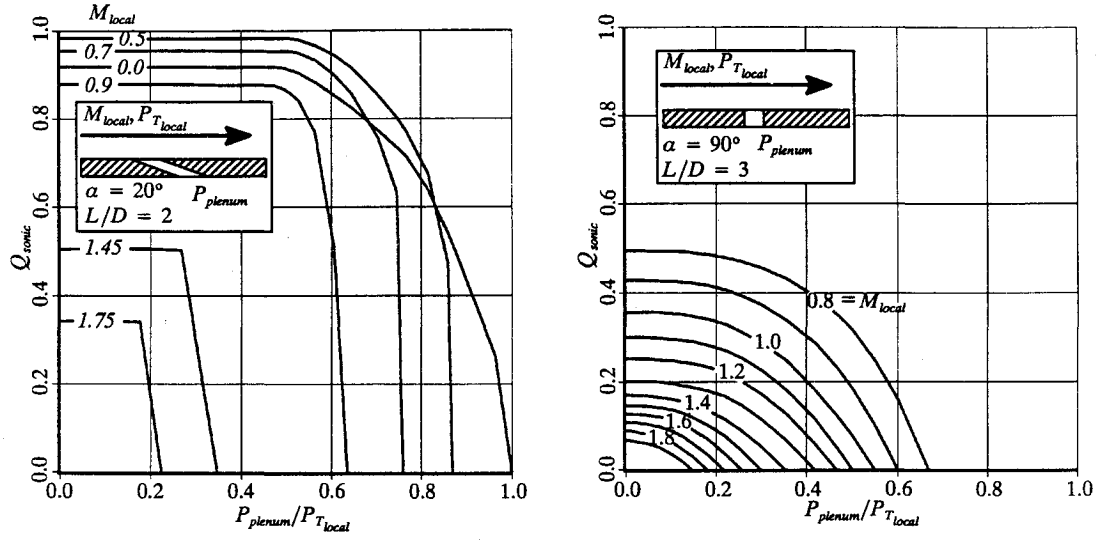

Fig. 2 Sonic mass flow coefficient data.

Next the wall velocity is computed. For viscous flows, a no-slip condition is imposed,

$$\boldsymbol{u}_{\text{wall}} = \mathbf{0}$$

For inviscid flows, the wall velocity is replaced by the velocity component that is tangent to the wall,

$$(\boldsymbol{u}_{\text{wall}} \cdot \boldsymbol{t}_{\text{wall}})\boldsymbol{t}_{\text{wall}} \Rightarrow \boldsymbol{u}_{\text{wall}}$$

Next the bleed hole sonic mass flow coefficient,[6] Q_{sonic} is determined as a function of the bleed hole angle, the bleed plenum pressure, and the local flow properties; Q_{sonic} is defined by

$$Q_{\text{sonic}} \equiv \frac{\dot{m}_{\text{actual}}}{\dot{m}_{\max}} = f\left(\alpha_{\text{bleed}}, M_{\text{local}}, \frac{P_{\text{plenum}}}{P_{T\,\text{local}}}\right) \tag{3}$$

where $\dot{m}_{\max}$ is the maximum theoretical flow at the local stagnation pressure and stagnation temperature. The local flow properties are taken at the wall for inviscid flows or from the grid point that is just beyond the edge of the boundary layer for viscous flows.

The data used in this study for 20-deg bleed holes[7] and 90-deg bleed holes[6] are shown in Fig. 2. These Q_{sonic} data are input as tables of values for discrete values of M_{local} and $P_{\text{plenum}}/P_{T\,\text{local}}$. Bilinear interpolation is used to calculate the appropriate values for Q_{sonic} as the solution develops. The present procedure can be easily extended to include the characteristics of bleed holes at other angles, entrance shapes, exit shapes, and length-to-diameter ratios by simply adding the appropriate tabular data.

The Q_{sonic} data were measured under steady-state operating conditions. Since Q_{sonic} data measured under unsteady operating conditions are unavailable, steady-state values are used as a reasonable first approximation. The applicability of steady-state data to unsteady flow must be evaluated. However, since the bleed flow rate through a given bleed band is generally very small compared with the flow through the entire inlet (i.e., on the order of less than 1% of the inlet capture flow), using steady-state data should yield meaningful results. Future work will extend the bleed boundary condition to account for time-varying bleed plenum pressures, which will further improve the accuracy for unsteady inlet analyses.

Based on the definition for Q_{sonic} and accounting for the surface porosity Φ, the effective bleed velocity magnitude is computed as follows:

$$|\boldsymbol{u}_{\text{bleed}}| = Q_{\text{sonic}} \frac{TP_{T_{\text{local}}}}{\sqrt{T_{T_{\text{local}}}}P} g(\gamma)\,\Phi$$

where

$$g(\gamma) = \left(1 + \frac{\gamma - 1}{2}\right)^{\frac{-(\gamma+1)}{2(\gamma-1)}}$$

The bleed flow is assumed to be normal to the flow domain boundary, therefore the bleed velocity vector is given by

$$\boldsymbol{u}_{\text{bleed}} = |\boldsymbol{u}_{\text{bleed}}|\boldsymbol{n}_{\text{wall}}$$

Now the velocity on the boundary is set to the vector sum of the wall velocity and the bleed velocity

$$\boldsymbol{u} = \boldsymbol{u}_{\text{wall}} + \boldsymbol{u}_{\text{bleed}}$$

completing the application of the bleed boundary condition.

Compressor Face Boundary Condition

Most Euler/Navier-Stokes codes provide a mechanism for specifying a fixed static pressure or mass flow at an outflow boundary. This type of boundary condition is not adequate for unsteady inlet analyses since the pressure and mass flow at the compressor face can change with time in response to an engine transient or a transient in the freestream flow. To address this problem, a new compressor face boundary condition has been developed.

In typical aircraft engines the flow is choked at one or more locations (typically in the turbine nozzles and the thrust nozzle throat). Therefore, the flow through the entire engine is limited, and for steady-state operation the corrected flow at the compressor face is directly proportional to the limiting Mach number in the choked portion of the engine (i.e., the corrected flow is fixed at the compressor face). Conversely, engine or freestream transients cause a change in corrected flow at the compressor face. The new boundary condition has been developed to account for these conditions by specification of the compressor face corrected mass flow $\dot{m}_c$, either as a constant or as a linear function of the stagnation conditions.

The engine face Mach number can be related to the mass flow per unit area by the formula for isentropic mass flow[8] (written in the nondimensional variables)

$$\frac{\dot{m}}{A} = \gamma \frac{P_T}{\sqrt{T_T}} \frac{M}{\{1 + [(\gamma - 1)/2]M^2\}^{[(\gamma+1)/2(\gamma-1)]}} \tag{4}$$

It is apparent that $\dot{m}$ is proportional to P_T and inversely proportional to $\sqrt{T_T}$. Therefore, at a given Mach number the mass flow will vary as the local stagnation conditions change.

The actual engine flow rate is typically referenced to the flow that occurs at a specified reference condition (typically static conditions at sea level). Using Eq. (4) to relate the mass flow at the reference conditions to the actual mass flow yields

$$\dot{m}_r = \dot{m}\frac{\sqrt{T_T/T_{T_r}}}{P_T/P_{T_r}} = \dot{m}\frac{\sqrt{\theta}}{\delta} \equiv \dot{m}_c \tag{5}$$

which is usually defined as the corrected mass flow since it is the actual mass flow corrected to the reference conditions for the same engine entrance Mach number (i.e., M_{CF}).

Equations (4) and (5) can be rewritten to yield

$$\frac{\dot{m}_c}{A} = \gamma\frac{P_{T_r}}{\sqrt{T_{T_r}}}\frac{M}{\{1+[(\gamma-1)/2]M^2\}^{[(\gamma+1)/2(\gamma-1)]}} \tag{6}$$

Since the reference conditions are fixed, it is evident that specifying a constant Mach number is equivalent to specifying a constant corrected mass flow per unit area.

Changes in the freestream conditions result in changes in the stagnation pressure and stagnation temperature at the compressor face and, therefore, changes in the corrected mass flow and the compressor face Mach number. To account for this effect, a linear function for changes in the corrected mass flow with changes in P_T and T_T is provided by

$$\frac{\Delta\dot{m}_c}{\dot{m}_c} = K_P\frac{\Delta P_T}{P_T} + K_T\frac{\Delta T_T}{T_T} \tag{7}$$

where K_P and K_T are empirical coefficients specific to a given engine and engine operating condition. This function is modeled after a function reported in Ref. 9 that accounts for changes in T_T only. Use of this function assumes that the engine mass flow instantly responds to the change in flow conditions.

The compressor face boundary condition is implemented in PARC in a manner similar to the subsonic outflow boundary condition in that the static pressure is set and the density and velocity are extrapolated from upstream. The static pressure is not set to a constant value but instead is adjusted at each time step based on the average stagnation pressure, average stagnation temperature, and average Mach number on the compressor face boundary. The objective is to update this pressure in a time-accurate manner so that the unsteady flow in the inlet can be accurately computed.

The basic solution procedure is as follows: First the dependent variables at time $n+1$ are determined on the boundary by extrapolation from the upstream grid point values at time $n-1$ and n using Eq. (1). Next the mass flux weighted average stagnation pressure $\bar{P}_T$ and stagnation temperature $\bar{T}_T$ is computed at time $n+1$ on the boundary using the following formula:

$$\bar{\phi}_T = \frac{\int \phi_T \rho \boldsymbol{u}\cdot \mathrm{d}\boldsymbol{A}}{\int \rho \boldsymbol{u}\cdot \mathrm{d}\boldsymbol{A}}$$

Next the average Mach number is either taken from the input data or computed from the specified corrected mass flow per unit area using Eq. (6). The corrected mass flow per unit area may be specified either as a constant value or computed from Eq. (7). The average static pressure is then computed:

$$\bar{P} = \bar{P}_T\left(1+\frac{\gamma-1}{2}\bar{M}_{CF}^2\right)^{-\frac{\gamma}{\gamma-1}}$$

The final step is to impose the static pressure on the boundary by updating the local stagnation energy using the following formula:

$$E = \frac{\bar{P}}{\gamma-1} + \frac{\rho}{2}\boldsymbol{u}\cdot\boldsymbol{u}$$

This new boundary condition provides a mechanism for conveniently specifying the corrected mass flux on an outflow boundary of a flowfield solution. The boundary condition can be used by specifying 1) the average Mach number over the boundary, 2) the corrected mass flow per unit area through the boundary, or 3) the corrected mass flow per unit area as a linear function of P_T and T_T (to more accurately represent the engine response to freestream disturbances such as velocity or thermal gusts).

Since the boundary condition can be used to specify the corrected mass flow per unit area, it can also be used to simulate the effects of choke plates or choked nozzles. An additional benefit for steady-state analyses is that the boundary condition is nonreflective when a constant average Mach number is specified (i.e., disturbances are allowed to leave through the boundary without reflecting back into the solution domain), which improves solution convergence for these calculations. Disturbances are expected to originate at the engine face when using the linear corrected mass flow function to simulate the engine face for unsteady inlet flows.

Results

The new boundary conditions have been demonstrated for an instantaneous decrease in the corrected mass flow at the compressor face of the axisymmetric mixed-compression inlet shown in Fig. 1. The inlet lines were lofted using the CATIA[10] computer-aided design system to define boundaries for the CFD grid. The computational grid for the cases reported in the present study was generated using the GRIDGEN2D[11] grid-generation program. The axisymmetric calculation was performed using four grid blocks with a total of 6069 grid points. A mesh sensitivity study was not performed since the objective was to develop and demonstrate the bleed and compressor face boundary conditions. Grid density does influence the accuracy of computed results and must be considered when performing design analyses.

Euler calculations were used instead of Navier-Stokes calculations since fewer grid points are necessary and larger time steps are allowed, resulting in less computer time and smaller memory requirements. Euler calculations are thought to provide useful initial design information. The Euler results must be tested against Navier-Stokes and experimental results to determine the extent to which the Euler analysis can be used with the bleed boundary condition.

Two cases were devised to study the movement of the normal shock over the throat bleed band as the compressor face Mach number M_{CF} changes and to illustrate the difference between 20- and 90-deg bleed hole configurations on the motion of the shock. The bleed hole angle for all bleed bands was assumed to be 20 deg except for the throat bleed band on the inner cowl surface (i.e., the aftmost bleed region on the cowl), which had 20-deg bleed hole angles for case 1 and 90-deg bleed hole angles for case 2.

The cowl slot was simulated by a porous wall section using the discharge coefficient data for 20-deg bleed holes. The hole area for the slot was adjusted so that the bleed rate through the cowl slot plus cowl region 4 matched the value reported in Ref. 3. Table 2 compares the bleed rates predicted by PARC with the values reported in Ref. 3 when the throat normal shock was downstream of all bleed regions. The differences between the bleed rates predicted with PARC and those reported in Ref. 3 are probably due to the Euler calculation (which results in full velocity profiles on the walls) and the absence of throat blockage effects that would occur with the actual viscous profiles. The agreement is felt to be acceptable for boundary condition verification purposes.

Demonstration Case 1—20-Deg Bleed Holes Used for Cowl Bleed Region 4

The bleed system for this case is described in Table 1. Note that all of the bleed regions have 20-deg bleed hole angles. The compressor face Mach number was fixed at 0.4167, and the calculation was run until a steady-state solution was achieved with the throat normal shock just downstream of the throat bleed regions. This steady-state result is identified as $t = 0.0$ s on subsequent figures. Figure 3 shows the Mach number contours in the vicinity of the throat. Figure 4 shows the Mach number distribution along the centerbody and cowl walls and along the centerline of the duct.

This steady-state result was used as the initial condition for the shock transient calculation. The compressor face Mach number

Table 2 Bleed rates

Bleed region	Ref. 3, $\dot{m}_{bleed}/\dot{m}_{lip}$	PARC, $\dot{m}_{bleed}/\dot{m}_{lip}$	Difference, %
Cowl 1	0.0031	0.0040	+29
Cowl 2	0.0037	0.0045	+22
Cowl 3	0.0046	0.0057	+24
Cowl slot and 4	0.0120	0.0119	−1
Centerbody 1 and 2	0.0097	0.0124	+28
Centerbody 3	0.0082	0.0104	+27

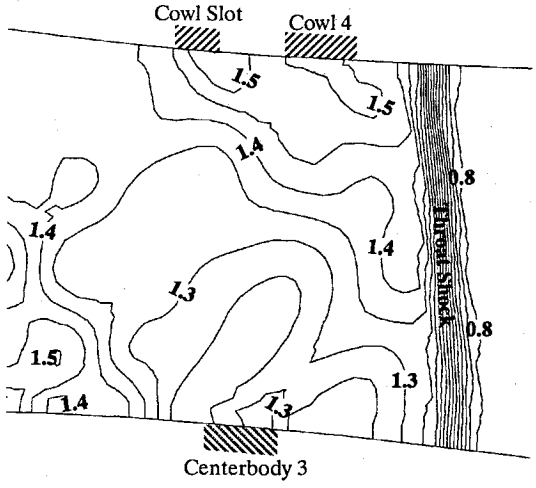

Fig. 3 Throat Mach contours with 20-deg bleed at t = 0.0 s.

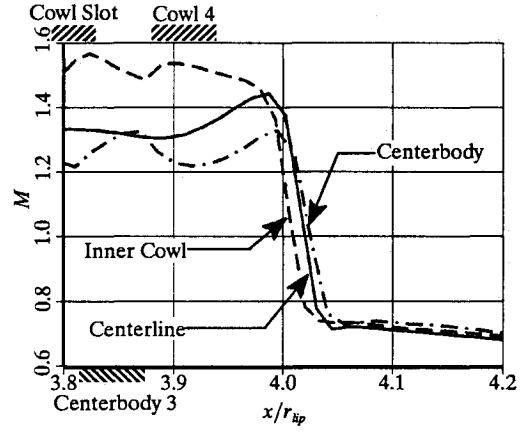

Fig. 4 Throat Mach distribution with 20-deg bleed at t = 0.0 s.

was reduced by 0.005 (to 0.4117, a 1.0% decrease in corrected mass flow), and a time-accurate solution was computed. The perturbation in the compressor face Mach number caused the throat normal shock to translate to the forward edge of the last bleed region on the cowl and onto the last centerbody bleed region. Mach number contours are shown in Fig. 5, and the Mach number distribution along the centerbody, cowl, and centerline is shown in Fig. 6.

The calculation was run with a fixed time step size of 5.54×10^{-5} s and a maximum Courant number of approximately 5.1. To translate the shock forward to the new steady-state condition, 1425 time steps were required. The elapsed time for this transient was 0.079 s. The calculation was performed on a Silicon Graphics 4D-35TG workstation and required 1.72 s of central processor unit (CPU) per time step.

The implicit residual smoothing option was used to allow calculation at a maximum Courant number of 5.1. Comparisons with calculations using a smaller maximum Courant number of 0.51 and without implicit residual smoothing have not revealed discernible differences in the steady-state results. The elapsed time for the shock transient was reduced by approximately 19%, however. Since a goal of the current study was prediction of the total forward translation of the normal shock, a maximum Courant number of 5.1 was used for most of the calculations reported in this article. In future studies aimed at a time-accurate simulation of the shock motion, a Courant number below 1 is thought to be necessary.

Demonstration Case 2—90-Deg Bleed Holes Used for Cowl Bleed Region 4

For this case the bleed system was nearly the same as for case 1 except that cowl bleed region 4 was modeled using 90- instead of 20-deg bleed hole angles. The flowfield for this configuration was computed to illustrate the effect of different bleed hole angles on the forward translation of the shock. To keep the same initial bleed rate as for Case 1, the bleed hole area for cowl region 4 was increased from 0.0076 to 0.0244 (i.e., the bleed hole porosity was increased by a factor of 3.2). This increase in bleed hole area was necessary to account for the decrease in the discharge coefficient. The initial condition was the same as shown in Figs. 3 and 4.

The same perturbation in compressor face Mach number was used to cause the shock translation (i.e., M_{CF} was decreased from 0.4167 to 0.4117). The calculation was run with the same time step size and Courant number as Case 1. The calculation required 1175 time steps to translate the shock forward to the new steady-state condition. The elapsed time for this transient was 0.065 s (a temporal error was undoubtedly introduced by allowing a maximum Courant number of 5.1) and required 1.73 s of CPU time per time step. Mach number contours are shown in Fig. 7, and the Mach number distribution is shown in Fig. 8.

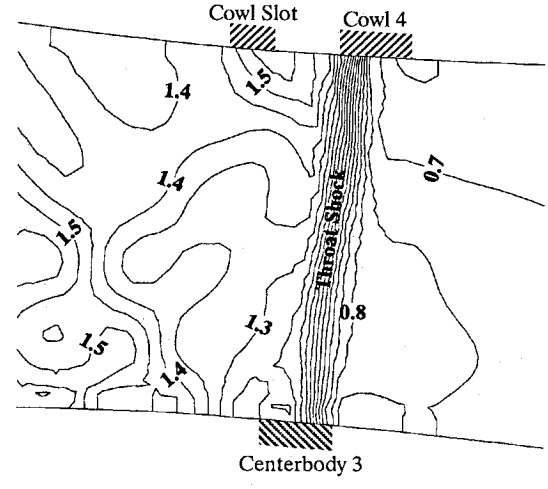

Fig. 5 Throat Mach contours with 20-deg bleed at t = 0.079 s.

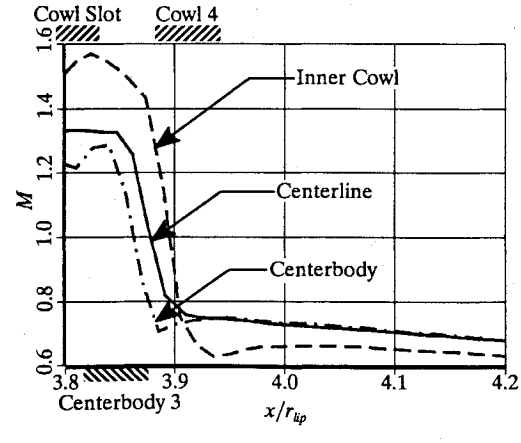

Fig. 6 Throat Mach distribution with 20-deg bleed at t = 0.079 s.

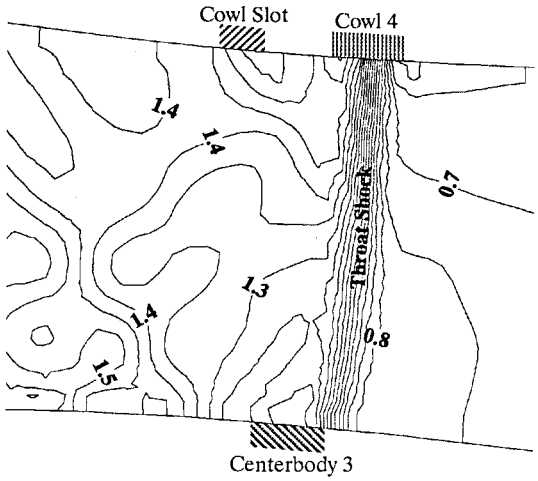

Fig. 7 Throat Mach contours with 90-deg bleed for cowl region 4 at t = 0.065 s.

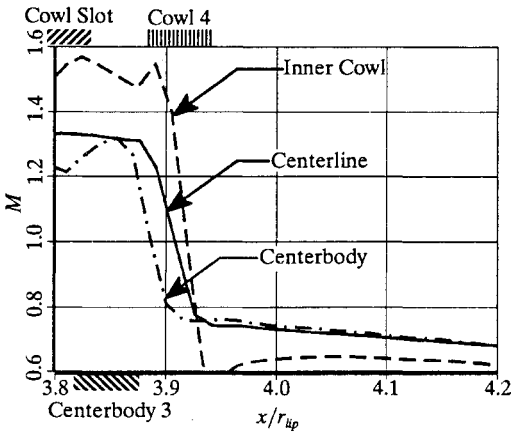

Fig. 8 Throat Mach distributions with 90-deg bleed for cowl region 4 at t = 0.065 s.

Note that the shock has not translated as far forward as in case 1. The normal shock has moved approximately halfway across cowl bleed region 4. The shock moved to the forward edge of region 4 in case 1. This indicates that using 90-deg bleed holes leads to an extra margin of stability for the inlet, since a greater change in engine mass flow can be tolerated before the inlet will unstart.

The stabilizing influence of bleed on the throat normal shock can be understood by examining Fig. 2 in conjunction with the following relationship developed by Paynter et al.[5]:

$$\frac{\mathrm{d}\,\dot{m}_{c_{CF}}}{\dot{m}_{c_{CF}}} + \frac{\mathrm{d}\,P_{T_{S2}}}{P_{T_{S2}}} + \frac{\dot{m}_{\text{bleed}}}{\dot{m}_{CF}} \frac{\mathrm{d}\,\dot{m}_{\text{bleed}}}{\dot{m}_{\text{bleed}}} = 0 \tag{8}$$

This formula shows that if the engine corrected mass flow decreases, this decrease must be offset by an increase in total pressure downstream of the shock (i.e., forward shock translation) and/or an increase in bleed mass flow. Figure 2 shows that for a given change in local Mach number a greater change in bleed mass flow occurs for 90-deg bleed holes than occurs for 20-deg bleed holes. Therefore, with the 90-deg bleed holes, less increase in $P_{T_{S2}}$ is required to satisfy Eq. (8), and this means reduced forward shock translation. This result is also consistent with the conclusions of Chyu et al.[1] that bleed boundary conditions that permit the bleed mass flow to change with the local flow properties have a more stabilizing influence on the throat shock than boundary conditions where the bleed mass flow is fixed.

Conclusions and Recommendations

The bleed and compressor face boundary conditions have been demonstrated with an analysis of the effects of a simulated engine transient on the flow in a typical supersonic inlet configuration. Validation of the use of Euler calculations for unsteady inlet analyses and the solution accuracy have not yet been performed but are required.

The test cases documented in this article demonstrate that 90-deg bleed holes in the throat region provide an extra margin of stability over 20-deg bleed holes. The bleed boundary condition currently sets the bleed hole discharge coefficient based on experimental data for either 20- or 90-deg bleed holes. Discharge coefficient data for additional bleed hole configurations can be easily added to the solution procedure.

Future work will focus on the following tasks:

1) Extend the bleed boundary condition to account for the temporal response of the bleed plenum pressure to changing bleed flow rates. This enhancement will improve the accuracy of the dynamic simulation of the inlet.

2) Extend the compressor face and bleed boundary conditions to three dimensions for use in the three-dimensional version of PARC.

3) Add a time-varying freestream condition to the PARC code so that the effects of freestream disturbances (e.g., thermal and velocity gusts) on inlet stability can be analyzed.

4) Run simulations with a maximum Courant number below 1 to examine the temporal response of the normal shock to either an upstream or downstream disturbance.

5) Perform viscous calculations to include throat viscous blockage effects (which affects the throat Mach number distribution, normal shock strength, and normal shock translation) and to improve the accuracy of bleed flow rate calculations.

Acknowledgments

The authors thank their colleagues at The Boeing Company, especially Chris Carlin, Joe Koncsek, Elling Tjonneland, and Dave Treiber, for valuable discussions on the subject of this article.

References

[1]Chyu, W. J., Howe, G. W., and Shih, T. I.-P., "Bleed Boundary Conditions for Numerically Simulated Mixed-Compression Supersonic Inlet Flow," *Journal of Propulsion and Power*, Vol. 8, No. 4, 1992, pp. 862–868.

[2]Abrahamson, K. W., and Brower, D. L., "An Empirical Boundary Condition for Numerical Simulation of Porous Plate Bleed Flows," AIAA Paper 88-0306, Jan. 1988.

[3]Syberg, J., "Analytic Design of AST Inlet," Boeing Co., D180-20551-1, Seattle, WA, March 1977.

[4]Cooper, G. K., and Sirbaugh, J. R., "PARC Code: Theory and Usage," Sverdrup Technology, Inc., AEDC-TR-89-15, Arnold Air Force Base, TN, Dec. 1989.

[5]Paynter, G. C., Mayer, D. W., and Tjonneland, E., "Flow Stability Issues in Supersonic Inlet Flow Analyses," AIAA Paper 93-0290, Jan. 1993.

[6]Syberg, J., and Hickcox, T. E., "Design of a Bleed System for a Mach 3.5 Inlet," NASA CR-2187, Sept. 1972, p. 33.

[7]McLafferty, G., and Ranard, E., "Pressure Losses and Flow Coefficients of Slanted Perforations Discharging from Within a Simulated Supersonic Inlet," United Aircraft Corp., Research Dept., R-0920-1, East Hartford, CT, Dec. 1958, p. 28.

[8]Shapiro, A. H., "The Dynamics and Thermodynamics of Compressible Fluid Flow," Vol. 1, Ronald Press Co., New York, 1953, p. 84.

[9]Barry, F. W., "Frequency of Supersonic Inlet Unstarts Due to Atmospheric Turbulence," NASA CR-137482, Oct. 1973.

[10]"CATIA Base Version 3, Interactive Functions Reference Manual," International Business Machines Corp., SH50-0098-05, Kingston, NY, Nov. 1991.

[11]Steinbrenner, J. P., Chawner, J. R., and Fouts, C. L., "The GRIDGEN 3D Multiple Block Grid Generation System," Vols. I and II, General Dynamics Corp., WRDC-TR-90-3022, Fort Worth, TX, July 1990.